Volume 9 | Number 34 | 14 September 2017 | Pages 12199–12758

Nanoscale

rsc.li/nanoscale

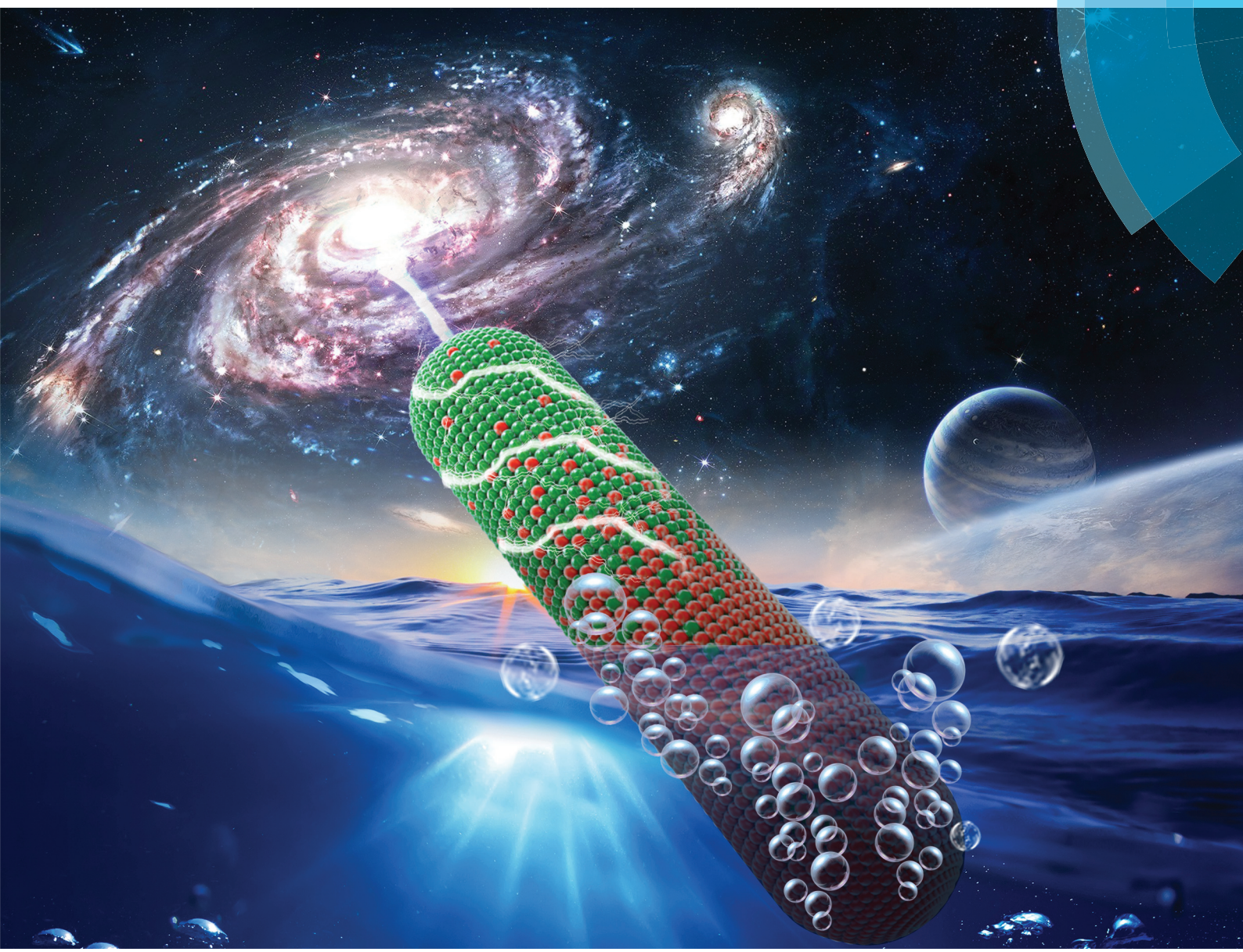

ISSN 2040-3372

ROYAL SOCIETY OF CHEMISTRY

PAPER

Bin Dong, Chen-Guang Liu *et al.*

In situ cathodic activation of V-incorporated Ni_xS_y nanowires for enhanced hydrogen evolution

NCNST

Nanoscale

PAPER

View Article Online
View Journal | View Issue

Published on 08 June 2017. Downloaded by China university of Petroleum (East China) on 8/20/2018 1:06:56 PM.

Check for updates

Cite this: *Nanoscale*, 2017, **9**, 12353

In situ cathodic activation of V-incorporated Ni_xS_y nanowires for enhanced hydrogen evolution†

Xiao Shang,[a] Kai-Li Yan,[a] Yi Rao,[a,b] Bin Dong,[a,b]* Jing-Qi Chi,[a] Yan-Ru Liu,[a] Xiao Li,[a] Yong-Ming Chai[a] and Chen-Guang Liu*[a]

Received 22nd April 2017,
Accepted 7th June 2017

DOI: 10.1039/c7nr02867a

rsc.li/nanoscale

In situ cathodic activation (ISCA) of V-incorporated Ni_xS_y nanowires supported on nickel foam (VS/Ni_xS_y/NF) can be realized in an alkaline hydrogen evolution reaction (HER) process, which provides not only clearly enhanced activity but also ultrahigh stability for HER. The ISCA process is continuous linear sweep voltammetry (LSV) on VS/Ni_xS_y/NF as a cathodic electrode with gradually enhanced HER activity. The activated VS/Ni_xS_y/NF (A-VS/Ni_xS_y/NF) demonstrates enhanced HER activity with an overpotential of 125 mV to drive 10 mA cm^{-2}, which is much lower than that of other samples. It may be predicted that the ISCA-derived amorphous VOOH film covering on A-VS/Ni_xS_y/NF accelerates the HER process, and NiOOH may protect active sites from decaying, leading to excellent activity and structural stability. However, for single metal sulfides, the ISCA process of nickel or vanadium sulfides is not available, implying that the synergistic effect between Ni and V of VS/Ni_xS_y/NF may be the key to drive ISCA in alkaline HER. In addition, its ultra-high stability confirms that the stable active sites and nanostructures of A-VS/Ni_xS_y/NF are derived from ISCA. Therefore, the ISCA of V-incorporated transition metal sulfides in the alkaline HER process may be a facile and promising method to obtain efficient electrocatalysts.

Introduction

Electrochemical water splitting has been considered as a sustainable method to obtain clean and renewable hydrogen fuel in recent years.[1–5] Full water splitting in alkaline media is highly attractive nowadays, which is advantageous to minimize overpotentials, simplifying the system and lowering cost.[3–5] At present, the most active catalysts for the hydrogen evolution reaction (HER) and oxygen evolution reaction (OER) in alkaline media are precious metals such as Pt- and Ir/Ru-based materials, respectively, which are impossible for widespread utilization.[6–8] Therefore, it promotes the development of earth-abundant electrocatalysts like low-cost Ni-based catalysts for water splitting,[9–14] represented by nickel sulfides with excellent electrocatalytic properties in alkaline.[15–19]

The enhanced activities of electrocatalysts for water splitting can be achieved by designing various nanostructures,[20,21] utilizing conductive substrates[20] and metal/non-metal doping.[22–27] Recently, facile and effective *in situ* electrochemical treatments such as *in situ* electrochemical tuning,[28] electrochemical activation,[29,30] electrochemical oxidation[31] and electrochemical etching[32,33] have been adopted to increase the active sites and stability during the OER process in alkaline solution. The enhanced activity and stability of electrocatalysts may be ascribed to *in situ* electrochemically-derived active species.[34–36] Cui's group has reported an *in situ* electrochemical oxidation (ISEO) tuning path to porous poor-crystalline transition metal oxides from transition metal sulfides with enhanced OER activity.[31,37] Our group has also demonstrated the efficacy of electrochemical oxidation to fabricate a highly active NiSe/NiOOH core–shell structure.[38] Furthermore, the synergistic effect in binary metal-based materials may be favorable for *in situ* electrochemical activation of surface active sites, such as Ni–V layered double hydroxide (LDH),[39] Ni–Co chalcogenides,[40] Ni–Co oxides[36] or Co–Fe phosphides.[35] Based on these previous studies, it can be inferred that *in situ* electrochemical activation may also be available in alkaline HER, whereas related research studies have been seldom reported.

Herein, we have achieved *in situ* cathodic activation (ISCA) of V-doped nickel sulfides on nickel foam (VS/Ni_xS_y/NF) during the HER process in alkaline solution, which suggests improved active sites and robust structures. The V-incorporation as well as the synergistic effect between Ni and V may drive the *in situ* cathodic surface activation in the HER process. The ISCA process is schematically illustrated in Scheme 1. With the addition of a V source in the hydrothermal process, VS/Ni_xS_y

[a]*State Key Laboratory of Heavy Oil Processing, China University of Petroleum (East China), Qingdao 266580, PR China. E-mail: dongbin@upc.edu.cn, cgliu@upc.edu.cn; Fax: +86-532-86981787; Tel: +86-532-86981376*

[b]*College of Science, China University of Petroleum (East China), Qingdao 266580, PR China*

†Electronic supplementary information (ESI) available. See DOI: 10.1039/c7nr02867a

Published on 08 June 2017. Downloaded by China university of Petroleum (East China) on 8/20/2018 1:06:56 PM.

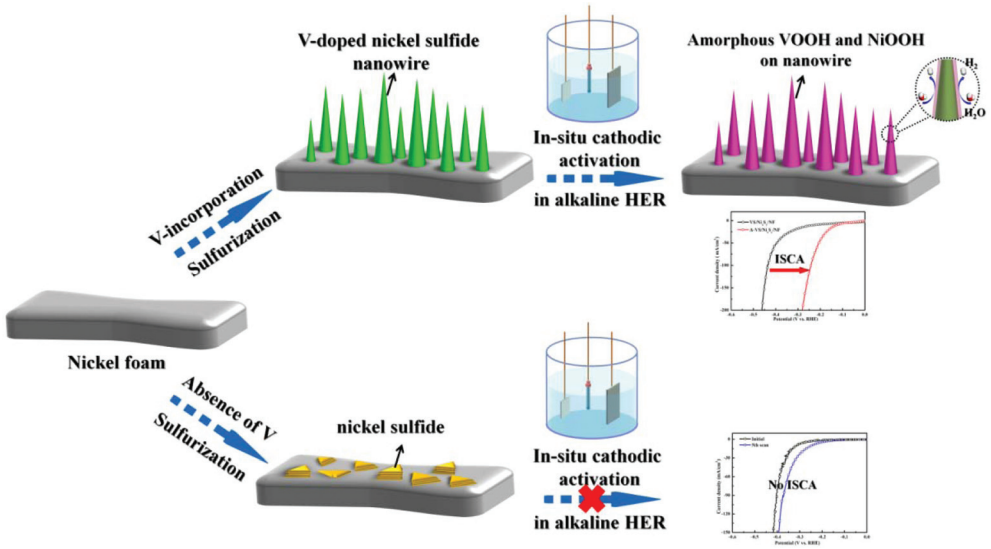

Scheme 1 Schematic representation of *in situ* cathodic activation (ISCA) of VS/Ni_xS_y/NF.

nanowire structures can be formed on NF. The nanowire structures may enlarge the surface area, expose more active sites and allow fast electrolyte diffusion to the active surfaces of the electrode. After ISCA (continuous linear sweep voltammetry scanning), the morphology of VS/Ni_xS_y nanowires remained unchanged, whereas *in situ* cathodic generated amorphous NiOOH and VOOH species can be detected on the surface of VS/Ni_xS_y nanowires by X-ray photoelectron spectra (XPS). The outer NiOOH and VOOH species greatly enhance HER activity and stability, while the inner VS/Ni_xS_y nanowires serve as a conductive scaffold for rapid charge transfer, stabilizing the surficial active species and preventing loss of their activity.[35] In contrast, the triangle-like nanosheets of nickel sulfide are formed on NF without V-incorporation. The ISCA process of single nickel sulfide can't be observed, which implies that the synergistic effect between Ni and V may be favorable for ISCA in alkaline HER.

Experimental section

All chemical reagents were of analytical grade as received without further purification. Nickel foam (NF, thickness of 1.0 mm, surface density of 350 g m^{-2}) was purchased from Shenzhen Poxon Machinery Technology Co., Ltd.

Synthesis of VS/Ni_xS_y/NF

Prior to the synthesis, NF was cut into 1 × 2 cm^2 and sonicated in acid, acetone and ethanol consecutively for 20 min, respectively. Then the clean NF was dried under vacuum at 60 °C for 8 h. In the typical synthesis of VS/Ni_xS_y/NF, 0.4132 g of thioacetamide was mixed with 0.1287 g of ammonium metavanadate in 40 mL of deionized water followed by vigorously stirring for 1.5 h to form a uniform light yellow solution. Then the solution was transferred into an autoclave (100 mL) with four pieces of NF at 160 °C for 24 h. After the autoclave was cooled down to room temperature naturally, as-prepared black products were carefully rinsed with deionized water and ethanol, and then dried under vacuum at 60 °C for 8 h. For comparison, Ni_3S_2/NF was prepared under the same conditions without the addition of ammonium metavanadate. The mass loadings of as-prepared samples have been roughly obtained by weight increment of NF after the synthesis of the active species on NF. For VS/Ni_xS_y/NF and Ni_3S_2/NF electrodes, the mass loadings were determined to be 13.5 mg cm^{-2} and 9.81 mg cm^{-2}, respectively.

Electrochemical activation

The *in situ* cathodic activation (ISCA) of VS/Ni_xS_y/NF on the cathode was carried out in 1.0 M KOH under a N_2 atmosphere to avoid possible oxidation caused by O_2 in air. This was conducted by using the three-electrode system of Gamry Reference 600 Instruments (USA). The as-prepared VS/Ni_xS_y/NF was used as the working electrode. A Pt foil and a saturated calomel (SCE) electrode were used as the counter and reference electrodes, respectively. The electrochemical cathodic activation was performed by linear sweep voltammetry (LSV) from −1.0 V to −1.5 V at least 20 times until the HER activity was stable. The *in situ* cathodic activated VS/Ni_xS_y/NF was named as A-VS/Ni_xS_y/NF.

Characterization

X-ray diffraction (XRD) patterns were recorded on an X'Pert PRO MPD diffractometer (Cu Kα) with a 2θ range from 10° to 75°. Scanning electron microscopy (SEM) measurements were performed on a Hitachi S-4800. X-ray fluorescence elemental analysis (EDX) was performed over a representative area of the as-prepared sample to identify the main elements on the surface. X-ray photoelectron spectra (XPS) were recorded on a ThermoFisher Scientific II spectrometer with Al as a photo source. Transmission electron microscopy (TEM) and high-

 This journal is © The Royal Society of Chemistry 2017

Published on 08 June 2017. Downloaded by China university of Petroleum (East China) on 8/20/2018 1:06:56 PM.

resolution transmission electron microscopy (HRTEM) images were recorded on a FEI Tecnai G2.

Electrochemical measurements

Electrocatalytic performances of as-prepared samples were measured using a three-electrode system (Gamry Reference 600 Instruments, USA). Typically, all as-prepared samples were used as the working electrodes. A carbon rod and a saturated calomel electrode were used as the counter and reference electrodes, respectively. All electrochemical data were recorded with iR (current time internal resistance) correction on Gamry Framework Data Acquisition Software 6.11. The electrolyte (1.0 M KOH) was degassed by N_2 in advance and N_2 was maintained above the solution during the HER measurement. LSV was conducted with a scan rate of 2 mV s^{-1}. Electrochemical impedance spectroscopy (EIS) was performed at −1.15 V (*vs.* SCE) from 10^5 to 0.01 Hz with an AC voltage of 5 mV. The double-layer capacitance (C_{dl}) was estimated by cyclic voltammetry (CV) data with various scan rates (40, 60, 80, 100 and 120 mV s^{-1}) from −0.7 to −0.9 V (*vs.* SCE). The stability tests were undertaken by cyclic voltammetry (CV) from −1.0 to −1.6 V (*vs.* SCE) or chronoamperometry at −1.3 V (*vs.* SCE). The potential conversion from SCE to reversible hydrogen electrode (RHE) is based on the equation as follows:

$$E\ (vs.\ \mathrm{RHE}) = E\ (vs.\ \mathrm{SCE}) + 0.244\ \mathrm{V} + (0.059\ \mathrm{V})\ \mathrm{pH}.$$

Results and discussion

The optical photographs of as-prepared Ni_3S_2/NF, VS/Ni_xS_y/NF and bare NF are displayed in Fig. S1.† The black color of VS/Ni_xS_y/NF, which is different from the gray color of Ni_3S_2/NF, implies the V-incorporation of VS/Ni_xS_y/NF. In order to detect the crystal structure of the as-prepared samples, the XRD patterns of Ni_3S_2/NF, VS/Ni_xS_y/NF are shown in Fig. 1. For Ni_3S_2/NF, all peaks detected can be well indexed to Ni_3S_2 (PDF no. 01-073-0698), indicating the successful preparation of Ni_3S_2/NF without any impurities. VS/Ni_xS_y/NF contains VS (PDF no. 96-900-8923) and mixed crystal Ni_xS_y (Ni_3S_2, PDF no. 01-073-0698; NiS PDF no. 03-065-2177), which suggests that V-incorporation may affect the growth of Ni_xS_y crystal phases.

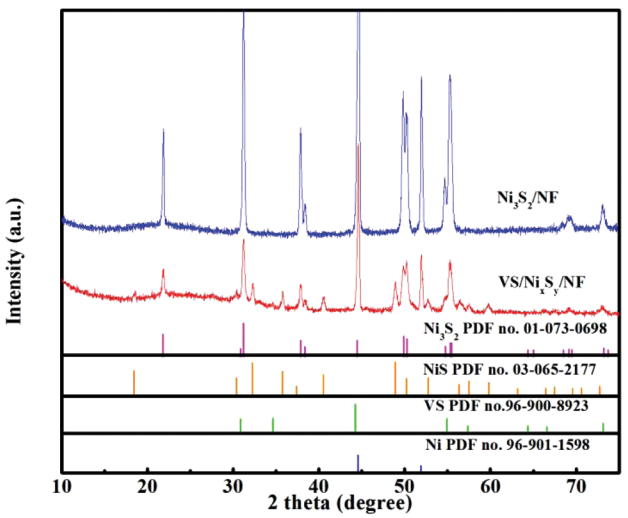

Fig. 1 XRD patterns of VS/Ni_xS_y/NF and Ni_3S_2/NF.

Compared with the smooth surface of bare NF (Fig. S2a†), Ni_3S_2/NF has a rough film (Fig. S3a†) on NF containing stacking of triangle-like nanosheets (Fig. S3b†). The stacking of triangle-like nanosheets can also be observed in the TEM image in Fig. S3c.† The HRTEM in Fig. S3d† shows the existence of (100), (110) and (210) facets belonging to Ni_3S_2. The selected area electron diffraction (SAED) shown in Fig. S3d† with the detection of (110) and (210) facets also demonstrates the formation of Ni_3S_2 on NF. With the addition of V, VS/Ni_xS_y/NF (Fig. 2a and b) contains a nanowire structure covering on NF uniformly. The transformation from triangle-like nanosheets to nanowires implies the effect of V-incorporation on the morphology of Ni_xS_y. The nanowire structure may be beneficial for mass transport and fast diffusion of the electrolyte during the electrocatalysis process. The TEM image in Fig. 2c shows that the VS/Ni_xS_y nanowire has an average diameter of 80 nm. The HRTEM image in Fig. 2d shows the facets of (110), (300) and (012) belonging to Ni_3S_2, NiS and VS, respectively. This indicates that the VS/Ni_xS_y nanowire is composed of mixed crystals of Ni_xS_y (Ni_3S_2 and NiS) and VS, consistent with a previous XRD analysis (Fig. 1). The successful incorporation of V can also be proved by the detection of the V element in EDX spectra (Fig. S4b†) compared with bare NF (Fig. S2b†) and Ni_3S_2/NF (Fig. S4a†). SEM mapping (Fig. S4c†) shows that the Ni, V, and S elements are uniformly distributed on the whole surface of VS/Ni_xS_y/NF. TEM mapping of a VS/Ni_xS_y nanowire scraped off the NF substrate (Fig. S4d†) confirms the uniform distribution of Ni, V, and S elements on a single VS/Ni_xS_y nanowire structure.

The *in situ* cathodic activation (ISCA) of VS/Ni_xS_y/NF is carried out in 1.0 M KOH under a N_2 atmosphere. The cathodic activation process of VS/Ni_xS_y/NF from the initial linear sweep voltammetry (LSV) to reach a stable state is shown in Fig. 3. In Fig. 3a, the initial VS/Ni_xS_y/NF shows low HER activity in alkaline requiring a large overpotential of 233 mV to reach 10 mA cm^{-2}. When reaching a stable state, A-VS/Ni_xS_y/NF only needs 125 mV to drive 10 mA cm^{-2}, illustrating greatly enhanced HER activity derived from ISCA. To compare the HER activities of VS/Ni_xS_y/NF before and after ISCA, the calculated values of electrochemically active surface area (ECSA) are provided in Table S1,† in which the value of ECSA can be estimated by positively-correlated electrochemical double-layer capacitance (C_{dl}) derived from the CV results (Fig. S5†). In Fig. 3b, A-VS/Ni_xS_y/NF shows an enhanced areal capacitance of 41.46 mF cm^{-2} about 2-fold higher than that (22.23 mF cm^{-2}) of VS/Ni_xS_y/NF. The enhanced ECSA of ISCA-derived A-VS/Ni_xS_y/NF strongly indicates the increased exposure of active sites for HER,[41,42] which proves the successful application of ISCA on Ni–V sulfides. The EIS data with a simplified equivalent circuit are shown in Fig. 3c to better understand the

Published on 08 June 2017. Downloaded by China university of Petroleum (East China) on 8/20/2018 1:06:56 PM.

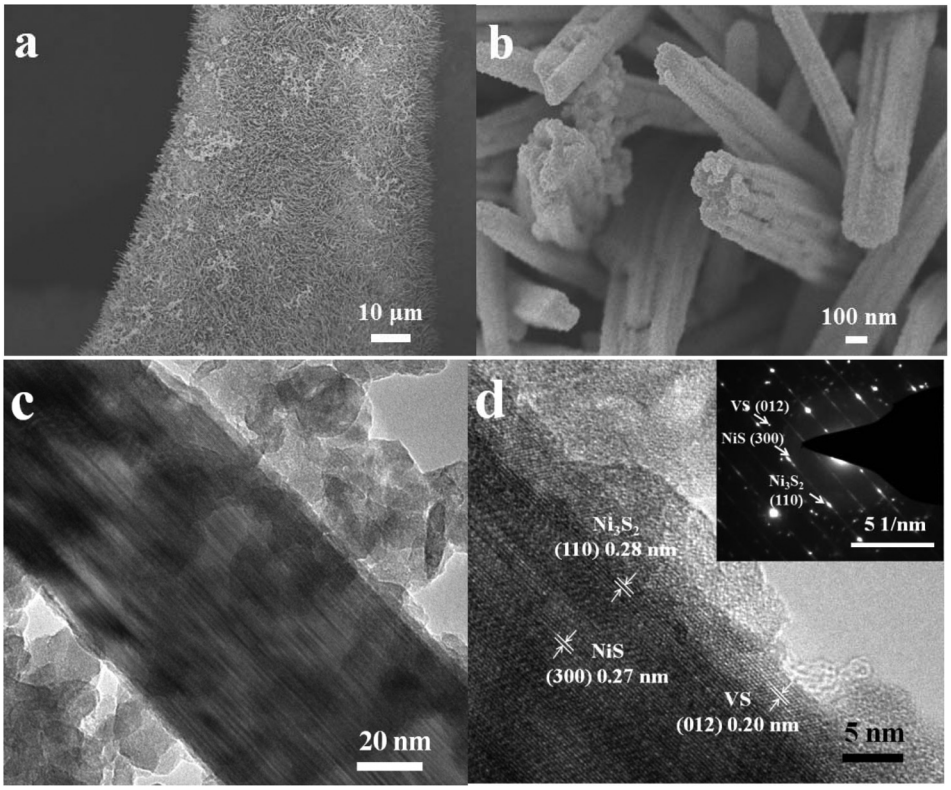

Fig. 2 (a, b) SEM images of VS/Ni_xS_y/NF. (c) TEM image and (d) high-resolution transmission electron microscopy (HRTEM) image of VS/Ni_xS_y/NF (insertion: selected area electron diffraction (SAED) of VS/Ni_xS_y/NF).

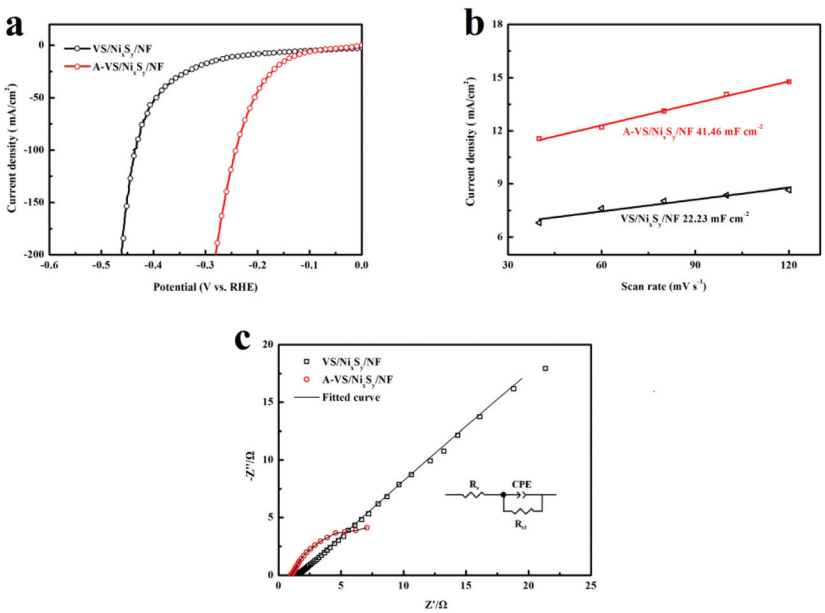

Fig. 3 *In situ* cathodic activation (ISCA) of VS/Ni_xS_y/NF. (a) Linear sweep voltammogram (LSV). (b) Determined double-layer capacitance (C_{dl}). (c) Electrochemical impedance spectroscopy (EIS).

 This journal is © The Royal Society of Chemistry 2017

Published on 08 June 2017. Downloaded by China university of Petroleum (East China) on 8/20/2018 1:06:56 PM.

charge transfer impendence. In this equivalent circuit, R_s is related to the electrical transport property of a catalyst, and CPE represents a constant phase element. The charge transfer resistance (R_{ct}) is associated with the catalytic kinetics at the catalyst/electrolyte interface. The sharply decreased diameter of A-VS/Ni_xS_y/NF in the Nyquist plots of Fig. 3c suggests a much faster electron-transfer kinetics of A-VS/Ni_xS_y/NF derived from ISCA. In addition, the corresponding R_{ct} (13.0 Ω) of A-VS/Ni_xS_y/NF is much smaller than that (952.0 Ω) of VS/Ni_xS_y/NF in Table S2.† Therefore, the enhanced HER activity of A-VS/Ni_xS_y/NF demonstrates the efficacy of ISCA, which contributes to significantly increased active sites and enhanced conductivity.

In order to confirm the mechanisms of ISCA on the enhanced HER activity in alkaline, some possible factors have been further investigated including alkaline media, nickel sulfide and vanadium sulfide. To exclude the influence of alkaline solution (1.0 M KOH), VS/Ni_xS_y/NF was immersed in 1.0 M KOH for 24 h (named as I-VS/Ni_xS_y/NF) under an Ar atmosphere to avoid possible oxidation caused by O_2 in air. Fig. S6a† shows that the low HER activity of I-VS/Ni_xS_y/NF at the first scan of the polarization curves is similar to that of initial VS/Ni_xS_y/NF, illustrating that the alkaline media can't contribute to the enhanced HER activity. To confirm the role of Ni_3S_2, the consecutive LSV process is also conducted on Ni_3S_2/NF, and HER activity (Fig. S6b†) only increases slightly (no more than 5 scans of LSV) before reaching stable activity. The chronoamperometry of 10^4 s (at an overpotential of 130 mV) for Ni_3S_2/NF (Fig. S6c†) does not show any obviously increased current density, either. This suggests that single transition metal sulfides such as Ni_3S_2 cannot be activated through the ISCA in alkaline. Similarly, the as-prepared VS powder without addition of NF in the hydrothermal process also shows low HER activity without any enhancement after the consecutive LSV scans in Fig. S6d.† Therefore, it can be concluded that the factors of alkaline media, single nickel sulfide or vanadium sulfide that lead to the enhanced HER activity of VS/Ni_xS_y can be excluded. This implies that the V incorporation-derived synergistic effect between Ni and V may drive ISCA during the HER process.[35,36]

The structures of I-VS/Ni_xS_y/NF and Ni_3S_2/NF after ISCA have further been investigated. Fig. S7a† shows that I-VS/Ni_xS_y/NF contains a similar film covering on NF. The magnified SEM image (Fig. S7b†) and TEM image (Fig. S7c†) show that I-VS/Ni_xS_y/NF contains similar nanowires after immersion in 1.0 M KOH solution. HRTEM (Fig. S7d†) shows the facets of (100), (110) and (012) indexed to Ni_3S_2, NiS and VS, respectively, illustrating that the mixed crystals of Ni_xS_y and VS are reserved in the VS/Ni_xS_y nanowire after immersion in alkaline media. The SAED shown in Fig. S7d† with detected facets of (110) from Ni_3S_2, (110) from NiS and (012) from VS also demonstrates that the nanowire still contains Ni_3S_2, NiS and VS species. TEM mapping (Fig. S7e†) proves the existence of Ni, V, and S elements on the VS/Ni_xS_y nanowire with homogeneous distribution. The SEM mapping (Fig. S8a†) and EDX spectrum (Fig. S8b†) of I-VS/Ni_xS_y/NF show that Ni, V, and S can be detected on the whole surface of I-VS/Ni_xS_y/NF with uniform distribution. All of the data above imply that alkaline solution may not change the nanowire structure of VS/Ni_xS_y. In addition, the XRD patterns shown in Fig. S11a† show that the crystal structures of VS/Ni_xS_y are not changed through immersion in alkaline media. Even after ISCA, VS/Ni_xS_y still contains Ni_3S_2, NiS and VS structures, which is identical to the previous XRD pattern of A-VS/Ni_xS_y/NF. For Ni_3S_2/NF after ISCA, the triangle-like nanosheets become irregular nanoparticles with smaller sizes (Fig. S9b†) on NF (Fig. S9a†). After chronoamperometry, the triangle-like nanosheets are invisible and also become smaller nanoparticles (Fig. S9d and S9e†). The decreased content of S and the increased content of O shown in the EDX spectrum after ISCA (Fig. S9c†) and chronoamperometry (Fig. S9f†) imply the formation of nickel oxide species in alkaline HER.[43] The smaller Ni_3S_2 nanoparticles after ISCA and chronoamperometry can be observed in TEM images in Fig. S10a and S10c,† respectively. However, some facets such as (100) from Ni_3S_2 can be observed by HRTEM (Fig. S10b† for ISCA and Fig. S10d† for chronoamperometry, respectively) with the corresponding insertions of SAED. XRD data (Fig. S11b†) of Ni_3S_2/NF after ISCA and chronoamperometry show an unchanged structure of Ni_3S_2 on NF. This suggests that ISCA may only change the morphology of Ni_3S_2/NF with an unchanged crystal structure of Ni_3S_2.

The valence states of I-VS/Ni_xS_y/NF and Ni_3S_2/NF after ISCA have been further investigated. The XPS survey of Fig. S12a† confirms the existence of Ni, V, and S in I-VS/Ni_xS_y/NF. The Ni 2p spectra (Fig. S12b†) show the formation of $Ni(OH)_2$ [44,45] after immersion in alkaline media overnight, which is also proved by the increased peak intensity of Ni–O in the O 1s region (Fig. S12e†). The disappearance of Ni(0) in I-VS/Ni_xS_y/NF can correspond to the decreased peak intensities of metallic Ni from NF in XRD (Fig. S11a†). In Fig. S12c,† the V $2p_{1/2}$ and V $2p_{3/2}$ peaks can be divided into two synthetic peaks of V(IV) and V(V) at higher binding energies, respectively, indicating the formation of oxidized V species through immersion in alkaline media. The oxidized V species can also be proved by V–O in Fig. S12e.† For S 2p spectra in Fig. S12d,† the decreased peak intensities of S $2p_{1/2}$, S $2p_{3/2}$ and V–S imply that nickel sulfides and vanadium sulfides are oxidized by alkaline media. The formation of SO_4^{2-} at *ca.* 168.2 eV suggests the oxidation of S to higher valence states.[23] The great loss of S may be responsible for the low HER activity of I-VS/Ni_xS_y/NF in Fig. S6.† The XPS data of Ni_3S_2/NF after ISCA and chronoamperometry are shown in Fig. S13.† The XPS survey in Fig. S13a† indicates that Ni, S, and O can be detected in Ni_3S_2/NF and Ni_3S_2/NF after ISCA and chronoamperometry. The Ni 2p in Fig. S13b† shows that Ni $2p_{3/2}$ (at 855.2 eV) and Ni $2p_{1/2}$ (at 872.7 eV) are indexed to Ni–S in Ni_3S_2.[20] After ISCA and chronoamperometry, all peak intensities in the Ni 2p region decrease. The disappearance of Ni(0) may be attributed to the oxidation of metallic Ni to $Ni(OH)_2$ in water solution.[46] This can also be proved by the appearance of $Ni(OH)_2$ at 855.6 and 873.2 eV.[47] The decreased peak intensity can also be observed in the S 2p region (Fig. S13c†), implying the partial destruction of nickel sulfide species after ISCA and chronoamperometry.

Published on 08 June 2017. Downloaded by China university of Petroleum (East China) on 8/20/2018 1:06:56 PM.

The structure of A-VS/Ni_xS_y/NF is studied by physical characterization, as shown in Fig. 4. The morphology of nanowire structures on A-VS/Ni_xS_y/NF (Fig. 4a and b) is retained with uniform distribution after ISCA compared with the initial VS/Ni_xS_y/NF (Fig. 2a and b), which is also advantageous for mass transfer and fast diffusion of the electrolyte in alkaline

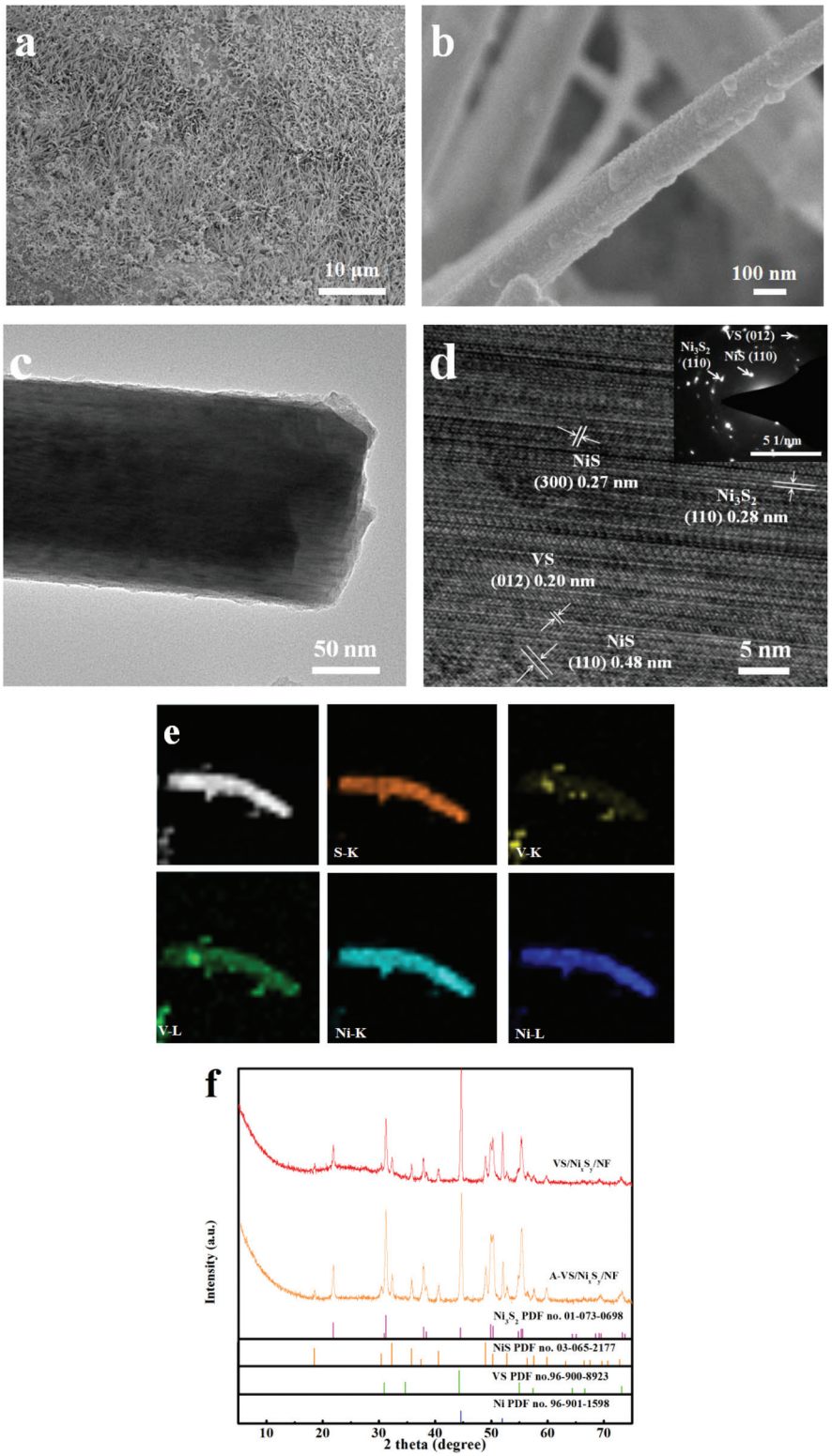

Fig. 4 (a, b) SEM images, (c) TEM and (d) HRTEM images of A-VS/Ni_xS_y/NF (insertion: the SAED of A-VS/Ni_xS_y/NF). (e) TEM mapping of the VS/Ni_xS_y nanowire in A-VS/Ni_xS_y/NF. (f) XRD patterns of VS/Ni_xS_y/NF and A-VS/Ni_xS_y/NF.

This journal is © The Royal Society of Chemistry 2017

Published on 08 June 2017. Downloaded by China university of Petroleum (East China) on 8/20/2018 1:06:56 PM.

HER. The corresponding TEM image (Fig. 4c) shows that the nanowire has an average diameter of 90 nm. In the HRTEM image (Fig. 4d), some facets such as (110) from Ni_3S_2, (110) and (300) from NiS, and (012) from VS can be observed. This demonstrates that the nanowire still contains Ni_3S_2, NiS and VS structures with a uniform distribution of Ni, V, and S in the nanowire (TEM mapping of Fig. 4e). However, the diameter of the VS/Ni_xS_y nanowire increased after activation. This unique phenomenon can also be observed in our previous work on enlarged NiSe nanocolumns.[38] In addition, no other new species can be found in the XRD patterns (Fig. 4f) for A-VS/Ni_xS_y/NF compared with those for VS/Ni_xS_y/NF, indicating that the ISCA process may not influence the crystal structure of A-VS/Ni_xS_y/NF. The decreased peak intensity of metallic Ni from NF may be caused by the conversion of metallic Ni to $Ni(OH)_2$ or NiOOH in alkaline media.[43,48] SEM mapping (Fig. S14a†) and the EDX spectrum (Fig. S14b†) show the existence of Ni, V, and S elements with uniform distribution on the whole surface of A-VS/Ni_xS_y/NF, implying that the ISCA process may not influence the distribution of Ni, V, and S elements on NF.

The A-VS/Ni_xS_y/NF has been further studied by XPS to reveal the influence of ISCA on the chemical states of VS/Ni_xS_y and how it influences the corresponding electrocatalytic activity. The XPS survey in Fig. 5a illustrates that Ni, V, and S elements can be found before and after ISCA. The detection of C and O suggests inevitable pollution and impurities.[49] For the Ni 2p orbit in Fig. 5b, the Ni $2p_{3/2}$ (at 855.2 eV) and Ni $2p_{1/2}$ (at 873.1 eV) are indexed to Ni–S in the mixed crystal phase of Ni_xS_y.[50] After ISCA, $Ni(OH)_2$ (855.6 eV and 873.2 eV)[47] and NiOOH (857.0 eV and 875.6 eV)[51] are detected. In comparison, the newly appeared peaks in the Ni 2p region of I-VS/Ni_xS_y/NF only contain $Ni(OH)_2$. Combined with a previous analysis of the low HER activity of I-VS/Ni_xS_y/NF (Fig. S6a†), this implies that alka-

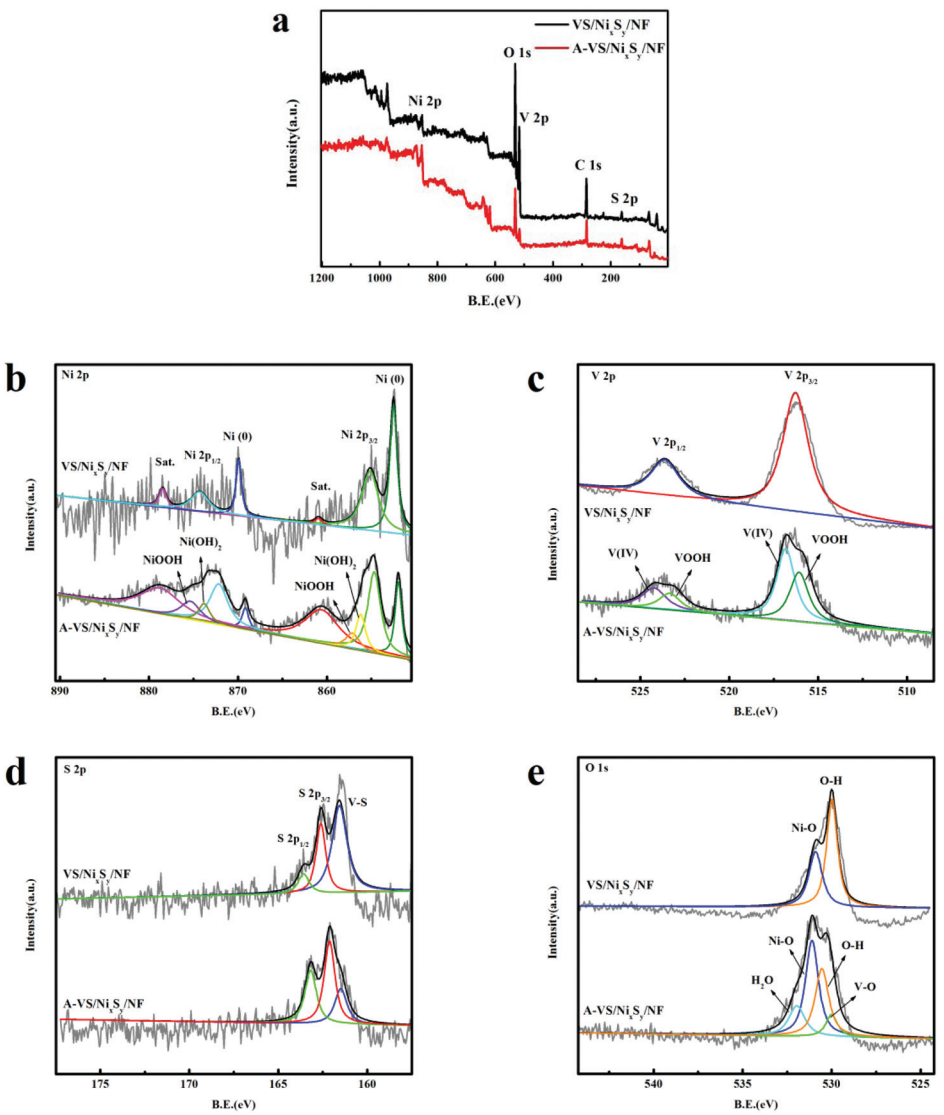

Fig. 5 XPS spectra of VS/Ni_xS_y/NF and A-VS/Ni_xS_y/NF. (a) Survey. (b) Ni 2p. (c) V 2p. (d) S 2p. (e) O 1s.

Published on 08 June 2017. Downloaded by China university of Petroleum (East China) on 8/20/2018 1:06:56 PM.

line media may not contribute to the enhanced HER activity. The increased intensity of the satellite peaks also illustrates the oxidation of nickel species.[52] In the V 2p region of Fig. 5c, the peaks at 516.3 and 524.1 eV indicate the oxidation of V(II) to V(IV).[53] The VOOH can be detected at 515.7 and 523.2 eV.[53] For the S 2p orbit in Fig. 5d, the weaker peak intensity of V–S at 160.6 eV (ref. 54) after ISCA implies the decreased content of V(II). Thus it can be inferred that the formation of VOOH in Fig. 5c may be from the conversion of V(II) to a higher oxidation state. In contrast, the alkaline media do not lead to the formation of VOOH on the surface of I-VS/Ni_xS_y/NF (Fig. S12c†) with low HER activity at the initial scan (Fig. S6a†). Due to the detection depth of XPS within a few nanometers, it can be speculated that the ISCA-generated VOOH species on the surface of the VS/Ni_xS_y nanowire may be ultrathin and serves as active sites for HER in alkaline.[55] Considering the generation of $Ni(OH)_2$ at the expense of the S element for I-VS/Ni_xS_y/NF as well as the corresponding low HER activity, it can be inferred that ISCA-generated NiOOH may protect sulfide species from corrosion in alkaline media. This confirms the efficacy of electrochemical activation on VS/Ni_xS_y/NF to produce abundant active sites such as amorphous VOOH on the surface of the VS/Ni_xS_y nanowire with amorphous NiOOH as protection. In Fig. S12d,† the S 2p peaks at 162.3 and 163.5 eV are from Ni–S bonds in VS/Ni_xS_y/NF.[56] In addition, a lower shift of binding energies of S 2p peaks through ISCA suggests the electron density transfer from Ni and V to S, which makes Ni and V positively charged, while S is negatively charged in A-VS/Ni_xS_y/NF.[10,57,58] The positively charged metal, namely the higher oxidation state of Ni and V, is believed to have better catalytic properties.[31,59–61] The O 1s region is shown in Fig. 5e. The peaks at 531.0 eV and 530.0 eV are derived from Ni–O and O–H, respectively.[45,55] The new appearance of V–O at 529.9 eV can be due to oxidation of V(II).[55]

The HER properties of A-VS/Ni_xS_y/NF and Ni_3S_2/NF are investigated in 1.0 M KOH in comparison with bare NF and commercial Pt/C, as shown in Fig. 6. In the LSV curves of Fig. 6a, Pt/C is the most active for alkaline HER with a low overpotential of 32 mV to deliver 10 mA cm^{-2}, while bare NF behaves poorly for HER. Compared with bare NF, Ni_3S_2/NF shows enhanced HER properties containing nickel sulfides as active species for HER. With the incorporation of V and the subsequent ISCA process, A-VS/Ni_xS_y/NF shows much better HER activity than Ni_3S_2/NF. A-VS/Ni_xS_y/NF requires an overpotential of 125 mV to drive 10 mA cm^{-2}, which is much lower than that (185 mV) of Ni_3S_2/NF. The alkaline HER kinetics have been further estimated by Tafel plots (Fig. 6b). The Tafel slopes for A-VS/Ni_xS_y/NF, Ni_3S_2/NF, bare NF and Pt/C are 113 mV dec^{-1}, 129 mV dec^{-1}, 133 mV dec^{-1} and 31 mV dec^{-1}, respectively. This indicates the improved HER reaction kinetics of A-VS/Ni_xS_y/NF compared to that of Ni_3S_2/NF. A further insight into the kinetics of alkaline HER of A-VS/Ni_xS_y/NF and Ni_3S_2/NF has been compared by EIS data (Fig. 6c). Through the equivalent circuit inserted in Fig. 6c, the fitting results of all samples are shown in Table S3.† The R_{ct} value of A-VS/Ni_xS_y/NF is the smallest (13.0 Ω), indicating the excellent conductivity of A-VS/Ni_xS_y/NF derived from high electron transfer efficiency. This suggests the effective ISCA process that results in an efficient Faradaic process and a superior HER kinetics under alkaline conditions. Moreover, the HER properties of

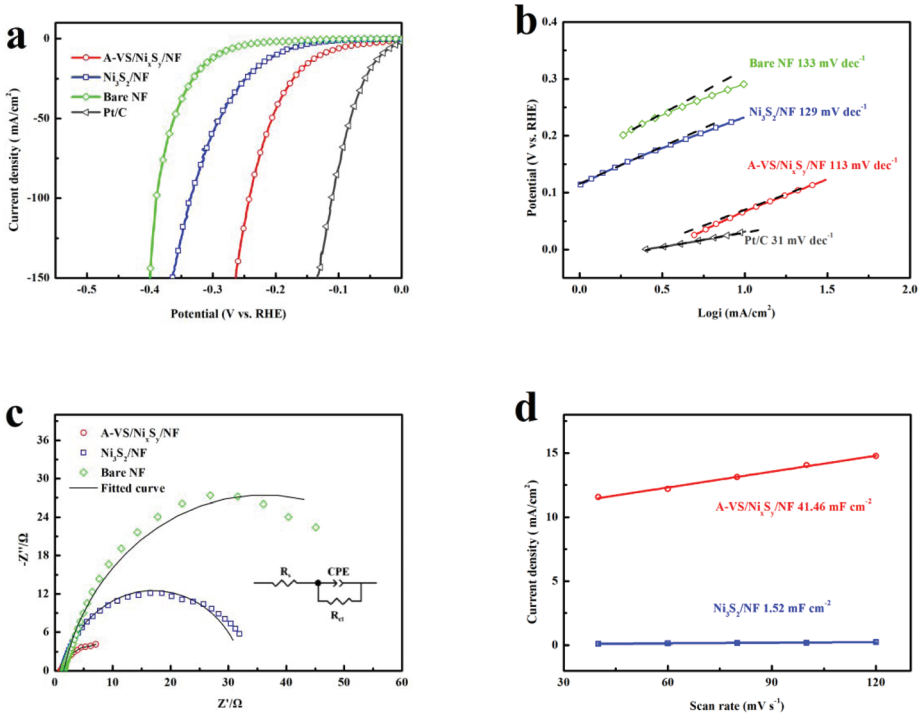

Fig. 6 Electrochemical measurements. (a) LSV. (b) Tafel plots. (c) EIS. (d) Determined C_{dl}.

This journal is © The Royal Society of Chemistry 2017

Published on 08 June 2017. Downloaded by China university of Petroleum (East China) on 8/20/2018 1:06:56 PM.

A-VS/Ni_xS_y/NF and Ni_3S_2/NF have been compared by ECSA. Through the corresponding CV results (Fig. S15 and Table S4†), the C_{dl} value of A-VS/Ni_xS_y/NF in Fig. 6d is determined to be 41.46 mF cm^{-2}, which is *ca.* 30-fold higher than that of Ni_3S_2/NF (1.52 mF cm^{-2}). The excellent HER activity of electrochemically activated A-VS/Ni_xS_y/NF is comparable to the highly active nickel sulfide-based electrocatalysts in 1.0 M KOH in recent work (Table S5†). The enhanced HER performance of A-VS/Ni_xS_y/NF may be caused by the incorporation of V into nickel sulfide to generate more active sites of VOOH on the surface proved by a previous XPS study (Fig. 5). Moreover, the larger ECSA of A-VS/Ni_xS_y/NF derived from ISCA indicates more exposure of active sites.[41,42] In addition, the increased oxidation states of Ni and V species may partially contribute to enhanced electrocatalytic activity.[60,62] This reveals that the incorporation of V may lead to a synergistic effect between Ni and V, which is favorable for ISCA.

To evaluate the catalytic stability of A-VS/Ni_xS_y/NF, long-term electrolysis has been carried out in 1.0 M KOH. In the CV test of Fig. 7a, A-VS/Ni_xS_y/NF can afford almost the same LSV curve as the initial catalyst with negligible cathode current drops after 6000 cycles. In the chronoamperometry measurement at an overpotential of 130 mV presented in Fig. 7b, the current density of A-VS/Ni_xS_y/NF exhibits slight degradation even after 12 h. All the stability tests demonstrate the excellent electrochemical stability toward the long-term HER process. The structures of A-VS/Ni_xS_y/NF after stability tests have been further investigated. As shown in Fig. 7c and d, the VS/Ni_xS_y nanowire structure remains unchanged after CV and chronoamperometry tests, respectively. In Fig. 7d, the surfaces of the nanowires are covered by a thin interwoven film that may be derived from the chronoamperometry process. The XRD results in Fig. S16† show that A-VS/Ni_xS_y/NF contains identical peaks of Ni_3S_2, NiS and VS after the stability tests, demonstrat-

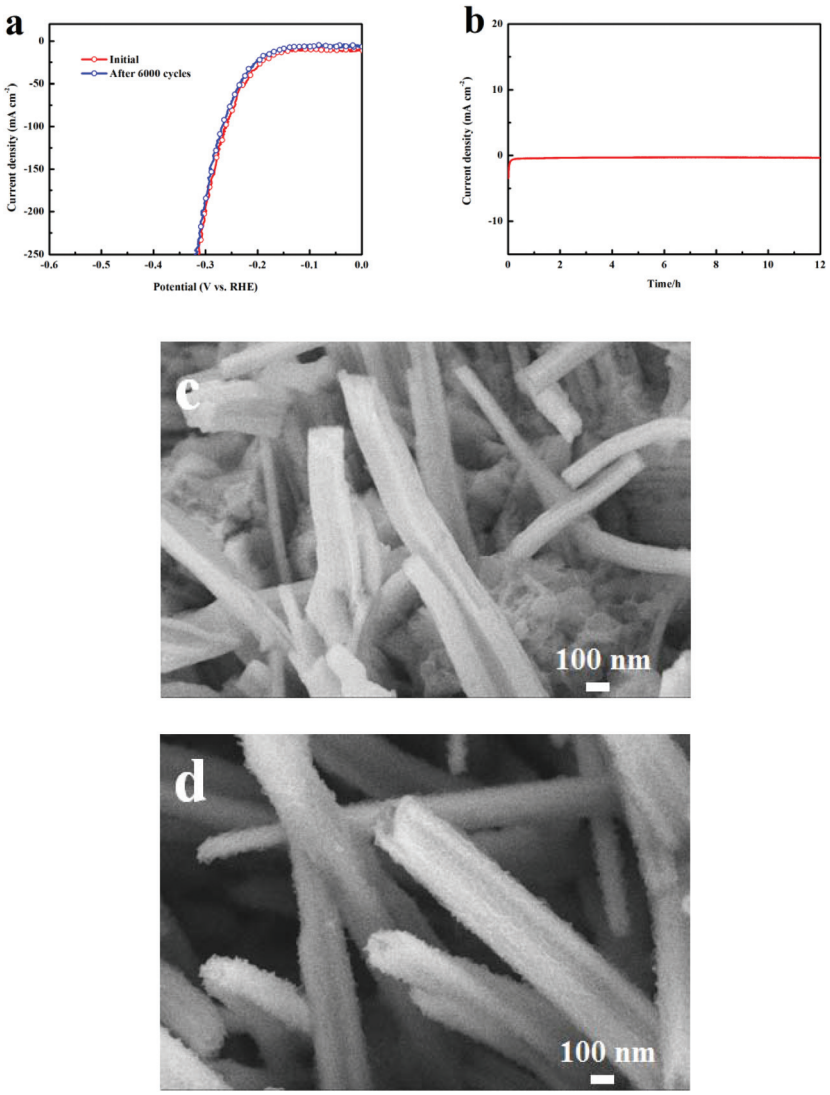

Fig. 7 Stability test of A-VS/Ni_xS_y/NF through (a) cyclic voltammetry (CV) and (b) 12 h chronoamperometry (at overpotential of 130 mV). SEM images of A-VS/Ni_xS_y/NF after the stability test through (c) CV and (d) 12 h chronoamperometry.

Published on 08 June 2017. Downloaded by China university of Petroleum (East China) on 8/20/2018 1:06:56 PM.

ing that all crystal structures in A-VS/Ni_xS_y/NF are well maintained. Under lower magnification (Fig. S17a and S17d†), the VS/Ni_xS_y the nanowires stay uniformly distributed on NF with unavoidable disappearance in small regions. The average diameter of the VS/Ni_xS_y nanowire after long-term electrolysis is 120–150 nm as observed in the TEM images after CV (Fig. S18a†) and chronoamperometry tests (Fig. S18d†). In SAED of Fig. S18b,† the facets of (110) and (210) from Ni_3S_2 and (300) from NiS and (012) from VS can be observed after the CV test, while the facets of (110) from Ni_3S_2, (101) from NiS and (012) from VS can be detected after the chronoamperometry test shown in Fig. S18e.† This illustrates that the VS/Ni_xS_y nanowires after the stability test still contain crystal structures of Ni_3S_2, NiS and VS. The SEM mappings of A-VS/Ni_xS_y/NF after the CV test (Fig. S17b†) and the chronoamperometry test (Fig. S17e†) with the corresponding TEM mappings (Fig. S18c and S18f,† respectively) show that the main elements of Ni, V, and S can still be uniformly dispersed on the surface of NF and VS/Ni_xS_y nanowires after long-term electrolysis. The EDX spectra in Fig. S17c and S17f† show that Ni, V, and S can be detected on the surface of NF after the stability test. However, the decreased content of V and S may be attributed to the possible loss of active sites during the long-term HER process. All physical characterizations suggest that ISCA-derived amorphous NiOOH may protect VS/Ni_xS_y from decay in alkaline media with a stable structure in long-term electrolysis.[35]

The valence states and the chemical environments of the main elements of A-VS/Ni_xS_y/NF after HER been evaluated by XPS, as shown in Fig. S19.† The XPS survey in Fig. S19a† illustrates that A-VS/Ni_xS_y/NF still contains Ni, V, and S elements after HER. The C and O detected in the survey suggest inevitable impurities in the characterization process. The higher magnification of Ni 2p (Fig. S19b†) and V 2p regions (Fig. S19c†) show the increased peak intensities of NiOOH and VOOH. This implies more conversion of nickel sulfide or vanadium sulfide to a higher oxidation state of NiOOH and VOOH, respectively. These conversions can also be observed in the lower peak intensity of S $2p_{3/2}$ and S $2p_{1/2}$ belonging to the Ni–S bond as well as the V–S bond in the S 2p region (Fig. S19d†). The increased content of NiOOH and VOOH after the stability tests can also be demonstrated in the increased peak intensities of Ni–O and V–O bonds shown in Fig. S19e.† All physical characterizations of A-VS/Ni_xS_y/NF after the stability test confirm the stable structure that maintains high performance for alkaline HER.

Conclusions

In summary, we developed *in situ* cathodic activation (ISCA) during an alkaline HER process for V-incorporated Ni_xS_y on NF (VS/Ni_xS_y/NF) with enhanced electrocatalytic activity. The ISCA-derived surficial amorphous VOOH and NiOOH on a VS/Ni_xS_y nanowire contribute to enhanced HER activity and structural stability, respectively. In contrast, ISCA of single nickel sulfide or vanadium sulfide cannot be realized, suggesting a possible synergistic effect caused by Ni and V, which is favorable for ISCA derived from alkaline HER. In addition, the *in situ* electrochemically activated VS/Ni_xS_y nanowire shows excellent stability in long-term HER of 6000 cycles with an unchanged nanowire structure. The ISCA-based binary transition metal sulfides through the alkaline HER process may provide a promising path to further enhance the electrochemical activity as well as structural stability.

Acknowledgements

This work is financially supported by the National Natural Science Foundation of China (U1662119) and the Fundamental Research Funds for the Central Universities (17CX06026 and 15CX05031A).

References

1 C. G. Morales-Guio, L.-A. Stern and X. Hu, *Chem. Soc. Rev.*, 2014, **43**, 6555–6569.
2 D. Yan, S. Dou, L. Tao, Z. J. Liu, Z. G. Liu, J. Huo and S. Y. Wang, *J. Mater. Chem. A*, 2016, **4**, 13726–13730.
3 X. Shang, W. H. Hu, X. Li, B. Dong, Y. R. Liu, G. Q. Han, Y. M. Chai and C. G. Liu, *Electrochim. Acta*, 2017, **224**, 25–31.
4 W. H. Hu, X. Shang, J. Xue, B. Dong, J. Q. Chi, G. Q. Han, Y. R. Liu, X. Li, K. L. Yan, Y. M. Chai and C. G. Liu, *Int. J. Hydrogen Energy*, 2017, **42**, 2088–2095.
5 C. Tang, N. Cheng, Z. Pu, W. Xing and X. Sun, *Angew. Chem., Int. Ed.*, 2015, **54**, 9351–9355.
6 W. H. Hu, G. Q. Han, Y. R. Liu, B. Dong, Y. M. Chai, Y. Q. Liu and C. G. Liu, *Int. J. Hydrogen Energy*, 2015, **40**, 6552–6558.
7 L. Yu, B. Y. Xia, X. Wang and X. W. Lou, *Adv. Mater.*, 2016, **28**, 92–97.
8 S. M. Tan and M. Pumera, *ACS Appl. Mater. Interfaces*, 2016, **8**, 3948–3957.
9 X. Li, X. Shang, Y. Rao, B. Dong, G. Q. Han, W. H. Hu, Y. R. Liu, K. L. Yan, J. Q. Chi, Y. M. Chai and C. G. Liu, *Appl. Surf. Sci.*, 2017, **396**, 1034–1043.
10 E. J. Popczun, J. R. McKone, C. G. Read, A. J. Biacchi, A. M. Wiltrout, N. S. Lewis and R. E. Schaak, *J. Am. Chem. Soc.*, 2013, **135**, 9267–9270.
11 G. Q. Han, Y. R. Liu, W. H. Hu, B. Dong, X. Li, X. Shang, Y. M. Chai, Y. Q. Liu and C. G. Liu, *Appl. Surf. Sci.*, 2015, **359**, 172–176.
12 Y. Wang, C. Xie, D. Liu, X. Huang, J. Huo and S. Y. Wang, *ACS Appl. Mater. Interfaces*, 2016, **8**, 18652–18657.
13 T. Liu, A. M. Asiri and X. Sun, *Nanoscale*, 2016, **8**, 3911–3915.
14 X. Liu, X. Wang, X. Yuan, W. Dong and F. Huang, *J. Mater. Chem. A*, 2016, **4**, 167–172.
15 B. Dong, X. Zhao, G. Q. Han, X. Li, X. Shang, Y. R. Liu, W. H. Hu, Y. M. Chai, H. Zhao and C. G. Liu, *J. Mater. Chem. A*, 2016, **4**, 13499–13508.

 This journal is © The Royal Society of Chemistry 2017

Published on 08 June 2017. Downloaded by China university of Petroleum (East China) on 8/20/2018 1:06:56 PM.

16 X. Y. Yu, L. Yu, H. B. Wu and X. W. D. Lou, *Angew. Chem., Int. Ed.*, 2015, **127**, 5421–5425.
17 L.-L. Feng, G. Yu, Y. Wu, G.-D. Li, H. Li, Y. Sun, T. Asefa, W. Chen and X. Zou, *J. Am. Chem. Soc.*, 2015, **137**, 14023–14026.
18 D. Y. Chung, J. W. Han, D. H. Lim, J. H. Jo, S. J. Yoo, H. Lee and Y. E. Sung, *Nanoscale*, 2015, **7**, 5157–5163.
19 Y. Wu, G. D. Li, Y. Liu, L. Yang, X. Lian, T. Asefa and X. Zou, *Adv. Funct. Mater.*, 2016, **26**, 4839–4847.
20 W. Zhou, X. J. Wu, X. Cao, X. Huang, C. Tan, J. Tian, H. Liu, J. Wang and H. Zhang, *Energy Environ. Sci.*, 2013, **6**, 2921–2924.
21 L. Xu, Q. Jiang, Z. Xiao, X. Li, J. Huo, S. Wang and L. Dai, *Angew. Chem., Int. Ed.*, 2016, **128**, 5363–5367.
22 Z. Cui, Y. Ge, H. Chu, R. Baines, P. Dong, J. Tang, Y. Yang, P. M. Ajayan, M. Ye and J. Shen, *J. Mater. Chem. A*, 2017, **5**, 1595–1602.
23 N. Cheng, Q. Liu, A. M. Asiri, W. Xing and X. Sun, *J. Mater. Chem. A*, 2015, **3**, 23207–23212.
24 J. Zhang and L. Dai, *Angew. Chem., Int. Ed.*, 2016, **128**, 13490–13494.
25 J. Zhang, L. Qu, G. Shi, J. Liu, J. Chen and L. Dai, *Angew. Chem., Int. Ed.*, 2016, **128**, 2270–2274.
26 J. Zhang, Z. Zhao, Z. Xia and L. Dai, *Nat. Nanotechnol.*, 2015, **10**, 444–452.
27 S. Dou, L. Tao, J. Huo, S. Wang and L. Dai, *Energy Environ. Sci.*, 2016, **9**, 1320–1326.
28 Y. Liu, H. Wang, D. Lin, C. Liu, P. C. Hsu, W. Liu, W. Chen and Y. Cui, *Energy Environ. Sci.*, 2015, **8**, 1719–1724.
29 H. Zhong, J. Wang, F. Meng and X. Zhang, *Angew. Chem., Int. Ed.*, 2016, **55**, 9937–9941.
30 F. Yan, C. Zhu, S. Wang, Y. Zhao, X. Zhang, C. Li and Y. Chen, *J. Mater. Chem. A*, 2016, **4**, 6048–6055.
31 W. Chen, H. Wang, Y. Li, Y. Liu, J. Sun, S. Lee, J.-S. Lee and Y. Cui, *ACS Cent. Sci.*, 2015, **1**, 244–251.
32 F. Song, K. Schenk and X. Hu, *Energy Environ. Sci.*, 2016, **9**, 473–477.
33 P. F. Liu, S. Yang, L. R. Zheng, B. Zhang and H. G. Yang, *J. Mater. Chem. A*, 2016, **4**, 9578–9584.
34 L. Xie, R. Zhang, L. Cui, D. Liu, S. Hao, Y. Ma, G. Du, A. M. Asiri and X. Sun, *Angew. Chem., Int. Ed.*, 2016, **56**, 1064–1068.
35 A. Mendoza-Garcia, D. Su and S. Sun, *Nanoscale*, 2016, **8**, 3244–3247.
36 M. Bajdich, M. García-Mota, A. Vojvodic, J. K. Nørskov and A. T. Bell, *J. Am. Chem. Soc.*, 2013, **135**, 13521–13530.
37 W. Chen, Y. Liu, Y. Li, J. Sun, Y. Qiu, C. Liu, G. Zhou and Y. Cui, *Nano Lett.*, 2016, **16**, 7588–7596.
38 X. Li, G. Q. Han, Y. R. Liu, B. Dong, W. H. Hu, X. Shang, Y. M. Chai and C. G. Liu, *ACS Appl. Mater. Interfaces*, 2016, **8**, 20057–20066.
39 K. Fan, H. Chen, Y. Ji, H. Huang, P. M. Claesson, Q. Daniel, B. Philippe, H. Rensmo, F. Li and Y. Luo, *Nat. Commun.*, 2016, **7**, 11981–11989.
40 C. Xia, Q. Jiang, C. Zhao, M. N. Hedhili and H. N. Alshareef, *Adv. Mater.*, 2016, **28**, 77–85.
41 J. Kibsgaard, Z. Chen, B. N. Reinecke and T. F. Jaramillo, *Nat. Mater.*, 2012, **11**, 963–969.
42 K. Xu, P. Chen, X. Li, Y. Tong, H. Ding, X. Wu, W. Chu, Z. Peng, C. Wu and Y. Xie, *J. Am. Chem. Soc.*, 2015, **137**, 4119–4125.
43 H. Yang, S. Luo, X. Li, S. Li, J. Jin and J. Ma, *J. Mater. Chem. A*, 2016, **4**, 18499–18508.
44 S. Xu, X. Lia, Z. Yang, T. Wang, M. Xu, L. Zhang, C. Yang, N. Hu, D. He and Y. Zhang, *Electrochim. Acta*, 2015, **182**, 464–473.
45 S. Xu, X. Li, Z. Yang, T. Wang, W. Jiang, C. Yang, S. Wang, N. Hu, H. Wei and Y. Zhang, *ACS Appl. Mater. Interfaces*, 2016, **8**, 27868–27876.
46 S. Ni, X. Lv, T. Li, X. Yang and L. Zhang, *J. Mater. Chem. A*, 2013, **1**, 1544–1547.
47 L. Wang, M. Li, Z. Huang, Y. Li, S. Qi, C. Yi and B. Yang, *J. Power Sources*, 2014, **264**, 282–289.
48 M. Ledendecker, S. Krick Calderón, C. Papp, H. P. Steinrück, M. Antonietti and M. Shalom, *Angew. Chem., Int. Ed.*, 2015, **54**, 12361–12365.
49 D. Merki, S. Fierro, H. Vrubel and X. Hu, *Chem. Sci.*, 2011, **2**, 1262–1267.
50 W. Kong, C. Lu, W. Zhang, J. Pu and Z. Wang, *J. Mater. Chem. A*, 2015, **3**, 12452–12460.
51 F. Zhang, D. Zhu, X. A. Chen, X. Xu, Z. Yang, C. Zou, K. Yang and S. Huang, *Phys. Chem. Chem. Phys.*, 2014, **16**, 4186–4192.
52 B. Konkena, J. Masa, A. J. Botz, I. Sinev, W. Xia, J. R. Koßmann, R. Drautz, M. Muhler and W. Schuhmann, *ACS Catal.*, 2016, **7**, 229–237.
53 Y. Xu, L. Zheng and Y. Xie, *Dalton Trans.*, 2010, **39**, 10729–10738.
54 C. S. Rout, B. H. Kim, X. Xu, J. Yang, H. Y. Jeong, D. Odkhuu, N. Park, J. Cho and H. S. Shin, *J. Am. Chem. Soc.*, 2013, **135**, 8720–8725.
55 H. Shi, H. Liang, F. Ming and Z. Wang, *Angew. Chem., Int. Ed.*, 2017, **129**, 588–592.
56 N. Jiang, L. Bogoev, M. Popova, S. Gul, J. Yano and Y. Sun, *J. Mater. Chem. A*, 2014, **2**, 19407–19414.
57 X. Wang, R. Tong, Y. Wang, H. Tao, Z. Zhang and H. Wang, *ACS Appl. Mater. Interfaces*, 2016, **8**, 34270–34279.
58 W. Kautek and J. G. Gordon, *J. Electrochem. Soc.*, 1990, **137**, 2672–2677.
59 M. R. Gao, Y. F. Xu, J. Jiang, Y. R. Zheng and S. H. Yu, *J. Am. Chem. Soc.*, 2012, **134**, 2930–2933.
60 J. G. McAlpin, Y. Surendranath, M. Dinca, T. A. Stich, S. A. Stoian, W. H. Casey, D. G. Nocera and R. D. Britt, *J. Am. Chem. Soc.*, 2010, **132**, 6882–6883.
61 J. B. Gerken, S. E. Shaner, R. C. Massé, N. J. Porubsky and S. S. Stahl, *Energy Environ. Sci.*, 2014, **7**, 2376–2382.
62 C. P. Plaisance and R. A. van Santen, *J. Am. Chem. Soc.*, 2015, **137**, 14660–14672.